Integrative Biology

Accepted Manuscript

ROYAL SOCIETY OF CHEMISTRY

www.rsc.org/ibiology

Insight, innovation, integration:

The effects of VEGF, a major regulator of vascular endothelial cells, have generally been studied using cells cultured on mechanically stiff polystyrene. However, vascular disease is associated with changes in blood vessel wall stiffness over a range that is significantly softer than tissue culture plastic. In this study, we explored how VEGF-induced calcium signaling in endothelial cells is modulated by the stiffness of the underlying substrate over a physiological relevant range (4-125 kPa). An image analysis tool was developed to allow us to quantitatively examine the response of individual cells, clusters of cells, and overall cell populations. We used this tool to identify distinctions in cells that responded most strongly to VEGF treatment as a function of stiffness.

Extracellular Matrix Stiffness Modulates VEGF Calcium Signaling in Endothelial Cells: Individual Cell and Population Analysis

Kelsey E. Derricks*, Vickery Trinkaus-Randall*^, Matthew A. Nugent`^

From the Departments of Medicine* and Biochemistry^ Boston University School of Medicine, 80 E Concord St. Boston, MA 02118

From the Department of Biological Sciences` University of Massachusetts Lowell, 198 Riverside St. Lowell, MA 01854

Address correspondence to: M. A. Nugent, Department of Biological Sciences, University of Massachusetts Lowell, Olsen Hall Room 414, 198 Riverside St. Lowell, MA 01854; Tel: 978-934-2860; Fax: 978-934-3044;

Supported in part by research grant M2012014 from the BrightFocus Foundation (MAN), NIH grant EY0600 (VTR), and a Departmental grant from the Massachusetts Lions Research Fund.

Running Title: ECM Stiffness Modulates VEGF Signaling

Key Words: Substrate stiffness, ECM, vascular endothelial growth factor, heterogeneous cell signaling, cell cluster analysis

Table of Contents Entry:

Endothelial cell responses to VEGF are heterogeneous and vary with ECM stiffness. We analyzed individual cell responses to VEGF as a function of substrate stiffness to identify unique clusters of cell signaling dynamics.

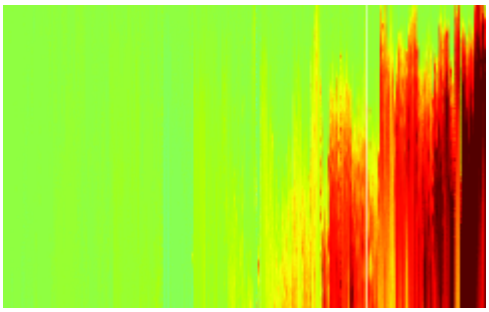

Abstract:

Vascular disease and its associated complications are the number one cause of death in the Western world. Both extracellular matrix stiffening and dysfunctional endothelial cells contribute to vascular disease. We examined endothelial cell calcium signaling in response to VEGF as a function of extracellular matrix stiffness. We developed a new analytical tool to analyze both population based and individual cell responses. Endothelial cells on soft substrates, 4 kPa, were the most responsive to VEGF, whereas cells on the 125 kPa substrates exhibited an attenuated response. Magnitude of activation, not the quantity of cells responding or the number of local maximums each cell experienced distinguished the responses. Individual cell analysis, across all treatments, identified two unique cell clusters. One cluster, containing most of the cells, exhibited minimal or slow calcium release. The remaining cell cluster had a rapid, high magnitude VEGF activation that ultimately defined the population based average calcium response. Interestingly, at low doses of VEGF, the high responding cell cluster contained smaller cells on average, suggesting that cell shape and size may be indicative of VEGF-sensitive endothelial cells. This study provides a new analytical tool to quantitatively analyze individual cell signaling response kinetics, that we have used to help uncover outcomes that are hidden within the average. The ability to selectively identify highly VEGF responsive cells within a population may lead to a better understanding of the specific phenotypic characteristics that define cell responsiveness, which could provide new insight for the development of targeted anti- and pro-angiogenic therapies.

Insight, innovation, integration:

The effects of VEGF, a major regulator of vascular endothelial cells, have generally been studied using cells cultured on mechanically stiff polystyrene. However, vascular disease is associated with changes in blood vessel wall stiffness over a range that is significantly softer than tissue culture plastic. In this study, we explored how VEGF-induced calcium signaling in endothelial cells is modulated by the stiffness of the underlying substrate over a physiological relevant range (4-125 kPa). An image analysis tool was developed to allow us to quantitatively examine the response of individual cells, clusters of cells, and overall cell populations. We used this tool to identify distinctions in cells that responded most strongly to VEGF treatment as a function of stiffness.

Introduction:

As humans and animals age, the vasculature of the body stiffens. The degree of stiffening correlates with cardiovascular morbidity, which can in turn lead to further stiffening pathologies such as atherosclerosis[1, 2]. The turnover of and alterations in the extracellular matrix (ECM) underlying the cells of the vasculature is largely responsible for this change. Disruption of the matrix metalloproteinase (MMP) balance and increased advanced glycation end products (AGE) contributes to increased collagen deposition, cross-linking, and subsequent stiffening of the vasculature[3-6]. How much the stiffness is altered in aging and disease is highly variable and may also depend on where the measurement was made. While healthy vessels range from about 2.5-50 kPa, diseased regions of vessels have stiffness ranges from about 10-200 kPa[7-10], and for comparison, tissue culture polystyrene stiffness is in the gigapascal range[11].

Various cell types respond to substrate stiffness differently. The fate of stem cells has been shown to vary depending on the ECM stiffness[12]. Confluent endothelial cells, without the aid of any growth factors, show increased permeability and proliferation as a function of the stiffness of the ECM on which they are cultured[13, 14]. Cells remodel and spread more extensively on stiffer substrates and the actin cytoskeleton increases its organization. However, substrate stiffness is not an independent stimulus to the cell as we have recently shown that the response of vascular smooth muscle cells to substrate stiffness is dependent on the specific matrix proteins present[14] and others have shown dramatically different endothelial cell responses to stiffness depending on specific source of the cells[15]. Cells have also been shown to take on the size and shape of the matrix beneath them[16]. An increase in protein ligand or stiffness results in a corollary increase in certain integrin proteins within mature focal adhesions[14, 17].

The ECM not only dictates cell adhesion properties, but also is a storage depot for growth factors. Fibronectin, a protein up-regulated in pathological conditions such as at sites of endothelial cell dysfunction, is well characterized as having a heparin binding domain where numerous growth factors can bind and potentially interact with cells[18-20]. Vascular endothelial growth factor (VEGF), a major pro-angiogenic protein, binds to fibronectin with a high affinity[18, 21, 22]. Prior studies have linked β1 integrin protein to matrix-bound VEGF and prolonged downstream signaling[23]. VEGF-receptor 2 activation, the

functional pathway responsible for much of VEGF biology, has been shown to cross react with several downstream integrin pathways, further suggesting a connection between the two receptor systems[24].

VEGF has been one of the most studied vasoactive agents as its potential to stimulate new vasculature and healing in areas damaged by age, wounds, or disease is widespread, yet attempts to use VEGF clinically have been unsuccessful likely due to a lack of complete understanding of its mechanism and effectors[25-27]. VEGF interacts with two main receptor types, VEGFR1 and VEGFR2. VEGFR1, has a high affinity for VEGF, storing the growth factor, blocking its interaction with VEGFR2[28]. VEGFR2 is responsible for downstream angiogenic properties such as vessel survival, migration, permeability, and proliferation. It signals through traditional tyrosine kinase receptor dimerization and activation of downstream effectors including ERK (proliferation), AKT (survival), and calcium flux (permeability)[28]. Endothelial cells have highly variable protein and epigenetic profiles based on the vascular bed of origin and even within an individual vessel. For instance, at any point an endothelial cell can be quiescent, or be involved in the angiogenesis process[29, 30]. An angiogenically active population of endothelial cells will send out an individual tip cell that is highly responsive to VEGF to initiate the migration and growth of a new capillary as directed by a matrix-bound VEGF gradient. Stalk cells, resting behind the tip cell, are also responsive to VEGF, but they proliferate rapidly to form the new vessel lumen[31, 32]. A better understanding of how to switch quiescent cells to angiogenic cells and *vice versa* could provide a pathway towards new treatment paradigms.

To test our hypothesis that ECM stiffness selectively modulates VEGF-endothelial cell activation, we developed a new analytical tool, which is able to uniquely access individual cell VEGF-calcium response and identify heterogeneous trends within a seemingly homogenous cell population. We found that response varied with stiffness in a complex manner. A large proportion of VEGF-treated cells were non-responsive or showed a slow, steady increase in activity, whereas a smaller subpopulation of highly responsive cells spiked rapidly and returned to a lower activation level. Response magnitude and rate, independent of stiffness depended on VEGF concentration. The highly responsive cells maintained a distinct shape indicating that primed, highly VEGF responsive, cells may have a shape-dependent

association. We present data that unmasks trends and populations previously hidden within a simple average.

Results:

The mechanical environment in which cells grow must be considered in a biological context. Growth factor availability and interactions vary with mechanical stiffening. To more fully appreciate how local mechanical properties impact growth factor activity, we devised an experimental system that allows cellular signaling kinetics to be monitored quantitatively using polyacrylamide gels of defined stiffness. Moreover, we developed an analytical approach that distinguishes the averaged response of a population of cells from the response of individual cells and clusters of cells. This approach will provide insight into the full range of growth factor activities within a biologically relevant context.

Our stiffness model consists of tunable polyacrylamide gels that are covalently linked to glass coverslips. The surfaces of the gels were exposed to a coverslip coated with Fn allowing passive transfer to occur during polymerization. Larger quantities of Fn were needed to functionalize the softer gels to produce gels that contained the same concentration of Fn on the surface (Figure 2A). The range of stiffness (4 - 125 kPa) was selected to represent reported values for normal and diseased vascular tissue *in vivo*[7-10]. In preliminary studies we attempted to extend this range to lower and higher stiffness values but observed alterations in the cells such that comparisons would involve multiple variables under these conditions. To verify that the ECM environments remained comparable after several days of cell exposure across the 4-125 kPa stiffness range, we imaged the Fn matrix on the three stiffness substrates after four days in culture and found no visible differences in the Fn fiber structure or density (Figure 2B). Additionally, we observed that the BAECs produce a varied ECM, which includes type 1 collagen (Figure 2B) after 3 days in culture. Thus, the mechanically tunable gel system provides a template to culture endothelial cells on in order to study the influence of matrix stiffness on cell behavior.

To study the cellular signaling response to VEGF and ECM stiffness, we measured the calcium response in endothelial cells cultured on gels of varying stiffness using live-cell imaging[33]. The individual cell analysis was conducted using a MATLAB script that is described in the methods section

(Figure 1). Analysis of 52 runs from multiple days, substrate stiffness, and treatment conditions indicate that the segmentation algorithm correctly identified cells 87% of the time.

The built-in functionality of MATLAB provided a way to quantify the average pixel intensities of every cell identified by the algorithm. Additionally, the major axis, minor axis, and area of each cell were quantified. Differences in the size and shape of the cells were analyzed on the various stiffness ECMs (Table 1). The changes in cell size, although significant, are not particularly large indicating that the BAECs are not especially sensitive to stiffness-modulated cell spreading under these conditions. We and others have shown that the specific ECM proteins present and the type of cells tested dictate the cell spreading response to stiffness[15, 34].

Numerous studies have investigated the various responses of endothelial cells to VEGF treatment. Many of these studies compile average readouts from a large population of cells using methods to measure mRNA and protein expression, or to measure cell responses such as cell proliferation, migration and tube formation. While these studies have defined important VEGF activities, it is likely that averaging the response over large populations of cells results in loss of pertinent information. To address these possibilities, while also exploring how substrate stiffness influences VEGF activity, we compared population base and individual cell analysis of the endothelial cell calcium response to VEGF to determine if ECM stiffness modulates VEGF responsiveness. We found minimal calcium mobilization in response to low doses of VEGF and attenuation of the response at high doses of VEGF treatment (Figure 3A). Maximal responses were observed with 5 ng/ml on 4 kPa ECM (1.5 and 1.7 fold over the 25 and 125 kPa samples, respectively) and 10 ng/ml on the 25 kPa ECM (1.6 and 1.8 fold over the 4 kPa samples and 125 kPa samples, respectively). The cellular response to VEGF on the 125 kPa ECM was insensitive to VEGF concentration, with the response showing little variation across the dose range analyzed.

To examine the dynamics of the average calcium response in greater detail, we computed a variety of outputs including maximal calcium response, rate of activation, and deactivation rate (parameters defined in Figure 4) for each of the conditions (VEGF dose and ECM stiffness) tested (Table

2). Table 2 also highlights the percent of cells that were activated for each treatment type for comparison to the normalized intensity values. The percent of cells activated was not dependent on concentration or stiffness and all alterations were minor compared to the magnitude of change in the normalized intensities. For example, although only 11% more cells responded in the 10 ng/ml treatment on the 25 kPa gels compared to the 4 kPa condition, there was a 43% increase in normalized intensity (Figure 3). There were no changes in the number of local maximums that each cell displayed across any stiffness. Together, these data indicate that the cells that responded in the 25 kPa condition responded with greater fortitude. Activation rates in the cells on 4 and 25 kPa matrices maintain a bell curve response with the maximum rate correlating with the maximal response, but on 125 kPa substrates, there was a concentration-dependent activation. This finding may indicate that a VEGF concentration leading to maximal activation in our 125 kPa condition was not met within our experiments. Simply, increasing doses of VEGF are necessary to maximally activate endothelial cells on stiffer substrates.

While population-based analysis can provide considerable insight into how cellular response varies with conditions, the fact that a large fraction (30-50%; Table 2) of the cells within the population did not become activated suggest that there might be considerably cell-to-cell variation that could impact the interpretation of the overall response. To compare and contrast the population-based average response to individual cell responses we utilized hierarchical clustering techniques to assess various portions of the clustering curves. In the hierarchical clustering scheme, we tested all the permutations of 8 distance measurements, 3 linkage measurements, and 5 different portions of the cell traces. The best clustering was completed with Seuclidean distances and average linkage analysis over only the peak activation time point (150 - 450 frames). Clustering accuracy was determined with a cophenetic correlation coefficient. The closer the coefficient is to 1, the more accurate the clustering scheme. All runs had coefficients of greater than 0.9.

The clustering scheme was utilized to organize cell traces of the peak frames (frames 150 - 450) into heatmaps (Figure 5). Dark maroon plots represent the highest activation and green represents no activation (positive or negative) as indicated by the heatmap scale. Each cluster that contained more than

three cells (with a cutoff value of 10 in the hierarchical tree) was plotted on a line graph presented under each corresponding heatmap. The average values were highlighted (bold blue line) and the largest individual cluster was also highlighted (bold gold lines). In every case the bulk of the cells (64-81%) had a response that was 1.7 to 8 fold less than that of the average response. The remaining cells, which were referred to as high responders, accounted for only 19-36% of the cells. The high responders had a magnitude of activation that was as much as 550% of the initial intensity in the highest response condition (25 kPa, 10 ng/ml VEGF).

To better examine how VEGF responses change with stiffness, we plotted the averages of all the normalized intensities for the overall average (thinnest lines within the middle), the bulk hierarchical cluster (thicker lines near the bottom) and the high responders not included in the bulk cluster (thick spiked lines on top) (Figure 6). The average intensity of the high responders was 73%-177% greater than the average normalized intensity value and 98-255% greater than the bulk cell response. The rate of activation of these clusters and the magnitude of response varied dramatically between the three different clusters of cells. Most of the cells (>50%) are activated in all conditions (Figure 3B), but showed a response of only 11-35% greater that the untreated values. Thus, the overall average response observed for all conditions was heavily weighted by the small fraction of cells that responded strongly to VEGF.

The kinetics and maximal responses of the three clusters are compiled in Table 3. The response of the bulk cluster was much more sustained than that of the high responders and the average response as indicated by the lower activation and deactivation rates and increased maximum time. For concentrations of VEGF below 25 ng/ml, cells on the 25 kPa and 125 kPa ECMs within the largest (bulk) cluster reached maximal response at the end of the treatment period (Figure 7). Activation and deactivation times, regardless of cluster, were almost always inversely correlated with concentration of VEGF. Activation time varied with VEGF dose suggesting that the rate of activation is likely a reflection of the time it takes for a threshold level of activated VEGF-VEGF receptor complexes to be reached, instead of being based on the intrinsic time required for signal processing. Faster activation rates also correlated with higher

maximum intensity values in almost all samples (except the average cluster on the 125 kPa ECM). The deactivation rate did not correlate with VEGF dose or ECM stiffness.

After segregating the cells into clusters based on normalized cell intensity, we wanted to explore how much variation remained in these after their extraction. We computed the coefficient of variation (COV; standard deviation/mean), for a variety of different parameters (Figure 8). We did not find any statistically significant differences among stiffness or VEGF concentration, but we did find that certain variables were much more predictable than others. We found that the maximum time and the overall area of the cells were the least variable (lower COV) as compared to the highly variable activation time and maximum values. When the high responders and bulk responders were analyzed separately we found significant differences in activation time, maximum time, and maximum values between these clusters. The differences were most notable for the high responder category, which has significantly reduced variability as compared to the bulk responders or to all the cells together. This suggests that cells in the high responder cluster are behaving in a more unified manner than the rest of the cell population, indicating that they may posses a characteristic that is predictive of VEGF responsiveness.

To determine if there are specific phenotypic characteristics among cells within a larger population that might indicate VEGF responsiveness, we compared specific cell shape parameters of the high responders to those of the bulk responders. Specifically, we compared the average cell area, and the major and minor axis lengths of the cells within the bulk responder cluster to those in the high responder cluster (Figure 9). At low concentrations of VEGF (1 ng and 5 ng/ml) we detected a significant decrease in overall cell area of the high responders. We also found a reduction in the minor and major axis lengths of the high responders in the 1 ng/ml VEGF treatment groups (Figure 9 A-C). The differences were no longer statistically significant in the groups that were treated with higher VEGF concentrations (10 and 25 ng/ml), and, as such, we observed that the differences in cell size between the two clusters were significantly reduced with increased VEGF concentration (Figure 9 D-F).

Variations in VEGFR2 levels on cells as a function of substrate stiffness and cell size/shape could provide a mechanism to explain the differences in VEGF responsiveness. To determine if VEGFR2

levels change under these conditions, flow cytometry analysis of our cells cultured on various stiffness substrates was performed. We observed consistent levels of VEGFR2 regardless of stiffness (Figure 10). Additionally, the forward scatter, a measure of relative cell size and the intensity of VEGFR2 staining only had a minor positive correlation with each other (average 0.55). Thus as cell size increases there may be a proportional increase in total VEGFR2 expression, indicating that receptor density does not vary with cell size.

Discussion:

Phenotypic changes in endothelial cells in response to stiffness have been well documented[15, 35-37], but little is known about how these changes impact intracellular signaling in response to external stimuli. In the present study we show that VEGF-induced calcium signaling within endothelial cells is modulated by stiffness. These changes in signaling were largely reflected by alterations in the magnitude of the cell response. The cells maintained the same number of local maxima, and the percentage of cells being activated was similar across the stiffness range evaluated. Interestingly, responses were attenuated in the cells on the stiffest substrates. Previous studies have shown specific integrin heterodimer expression increases with matrix stiffness[14, 38], suggesting a molecular mechanism by which cell-ECM engagement may be modulated by substrate stiffness. The mechanism of action of VEGF has been linked to the state of the extracellular matrix in a number of studies. Prior studies have assessed the ability of VEGF to interact with a variety of different ECM proteins including fibronectin[18, 19, 39]. Binding of VEGF to the matrix can extend downstream MAPK activation[22, 23]. In prior studies testing the binding ability of VEGF to various different ECM proteins, including type 1 collagen, VEGF bound with the greatest affinity to Fn[40]. Thus, although we have a variety of matrix proteins present (Figure 2), we hypothesize VEGF-Fn binding is likely involved in our differential VEGF signaling. Future studies can explore how specific ECM proteins might modulate VEGF response to stiffness.

VEGFR2 signaling has been shown to coordinate with integrin signaling, and physical association of VEGFR2 with integrins has been suggested to modulate VEGF internalization and

signaling kinetics[23, 28, 41-46]. Thus, the intimate connection between the VEGF system and the process by which the cell interacts with the ECM may provide the basis for how VEGF signaling is modulated by ECM stiffness.

The attenuation of VEGF signaling that we observed in cells on the stiffest matrices may relate to the inability of the body to repair severely stiffened atherosclerotic blood vessels as well as the ability of newly developing soft tissues and tumors to actively recruit the development and growth of new vasculature. The stiffness of diseased vessels can vary up to an order of magnitude, which can lead to dramatically altered cell phenotypes[7-9]. Primary cell cultures lose up to 40% of their microenvironment specific phenotypes when they are cultured on plastic[30, 47]. Thus, the use of cell culture substrates at more physiologically relevant stiffness may provide important insight into how cell response is controlled *in vivo*.

While our study revealed interesting distinctions in the response of endothelial cells to VEGF as a function of stiffness when averaged over the entire population, the power of our study was largely in the individual cell analysis. Prior studies have looked at endothelial cell heterogeneity[29, 30, 47, 48]. In particular, studies have explored how phenotypes, genetic, and epigenetic alterations occur in different vascular beds throughout the body. The size of cells, orientation of the cells, receptor densities, and immune system properties vary as a function of the specific vascular bed. Even within a single population of cells in one vascular bed, cells are known to dynamically change their behavior from quiescent to tip cell to stalk cell[29, 30, 47, 48]. In the present analysis we found that individual cell responses differ dramatically within a single population of cells in a well-controlled culture system. Thus, cell-to-cell variability may be an intrinsic property of endothelial cells that reflects a natural ability to exist in distinct phenotypic states. It is not clear from our analysis if the property of being highly sensitive to VEGF-induced signaling is a stable characteristic of a select group of cells within the population or a transient property that all cells posses under some conditions. Nevertheless, the ability to identify the relative proportion of sensitive cells as a means to accurately predict VEGF responsiveness in endothelial cells within specific environments *in vivo* could lead to new directed treatment avenues or cell models.

The kinetics of cellular response to external stimuli such as growth factors have been evaluated by measuring binding and signaling kinetics averaged over a large population of cells using biochemical methods, or analyzed in a select number of cells generally using microscopic techniques. Until recently, high order, individual cell dynamics and patterns were not explored. With the availability of new computational methods it is now possible to individually analyze fields of cells compiling millions of individual data points to answer a question. These techniques will be invaluable in deciphering how distinct growth factors can have such diverse endpoint responses while sharing many of the same signaling components. It is likely that cellular response is ultimately dictated by the sequence, timing, duration, and frequency of signal activation. Thus, it will be critical to develop tools to quantitatively track the dynamics of individual cell response in order to eventually decode cell behavior. For example, P53 protein levels oscillate with set frequency and amplitude after cell exposure to γ-radiation, but there is a concentration dependent persistent response after UV radiation[49]. In PC12 cells, epidermal growth factor induces transient ERK activation while nerve growth factor leads to a sustained ERK response, a response that may be essential for cell differentiation[50-52]. In other instances, the amplitude from baseline, not the timing, dictates the specific ERK activation[53]. Uncovering the role of signal dynamics in endothelial cells could provide further insight into activation and targets for inducing/eliminating angiogenesis.

The dynamics of calcium signaling have been shown to control individual cell fates. For example, transient spikes in calcium have been shown to activate different transcription factors than a sustained response[54, 55]. It is well known that VEGF activates calcium signaling through both phospholipase C IP_3-mediated release of intracellular calcium stores and TRPC3 and TRPC6 cation channels, but individual cell calcium response to VEGF has not been explored previously. We used a non-biased hierarchical clustering scheme to identify several distinct clusters. Analyzing these responses together as the bulk response and comparing it to remaining cells, or high responders, yielded some interesting findings. We found that temporal speed is a sensor for concentration. In general, as the concentration of VEGF increased, regardless of stiffness, we found a shortening of the time until

activation and time until the overall maximum point was reached. This finding indicates that activation time is not fully dependent on the reaction time, but instead likely reflects a threshold reaction whereby signaling is activated when a specified concentration of ligand-receptor complexes is reached.

While parsing out the individual cell response we were able to determine that endothelial cells on the softest substrates (4 kPa) were most sensitive to VEGF treatment. The percentage of high responders was altered by stiffness, but not in any discernable pattern. For example, in the 1 ng/ml VEGF condition, 19% of cells on the 4 kPa substrates, 29% of cells on the 25 kPa substrates and 35 % of the cells on the 125 kPa substrates were high responders. Despite those differences, the average of maximums of the high responders from each run in the 4 kPa condition was greater than that of either remaining stiffness indicating the active cells that were responding were stimulated to a greater extend than in the other stiffness conditions. High responders for the 4 kPa condition also had a greater difference between their high responders average maximum and bulk responders average maximum than in the other conditions. These trends were clear when looking at individual cell responses, but were not detectable within the average of the population-based responses.

Cells on our 25 kPa constructs (our model for a moderately aged vessel) had the greatest overall maximum and activation rate compared to any other condition, but this occurred at a moderate VEGF dose. It is possible that the integrin connection, or another biological pathway, is limiting the ability of the cells to respond to VEGF as stiffness increases. At the maximal VEGF dose tested, the difference in average maximum values of the high responders and bulk responders with substrate stiffness was lost. This indicates that the stiffness limitations to VEGF dose are overcome.

Our clustering analysis revealed some interesting conclusions regarding variability within the overall cell population. We found that ~40% of the cells did not respond at all regardless of stiffness and VEGF dose. In addition to the non-responders there were an additional 15-35% of cells that showed a slow muted response. The high responder group had a rapid, large, and transient increase in calcium release. Two distinct patterns of VEGF responsiveness that we detected have been reported previously. The Chen group reported two main clusters of traction force strain curves after VEGF treatment of

endothelial cells[56]. They treated endothelial cells with a range of VEGF doses and found that most cells exhibited no response or a gradual increase in strain energy when treated with lower concentrations (10 ng/ml) of VEGF, but as VEGF dose increased (up to 100 ng/ml), the number of cells displaying an initial spike of strain energy after VEGF treatment increased[56]. The high responders in our data set as an average have a peak response at 10 ng/ml, but closer examination of the heatmaps (Figure 5) shows that even though the average responses decreased at 25 ng/ml, there are more of the high responders exhibiting spikes as indicated by the increase in yellow lines. The similarities in dynamics and quantity of cells responding between our study and the Chen study may indicate that our high responders represent cells that have a migratory phenotype.

Only a fraction of the cells within the population responded strongly to VEGF suggesting that there may be differences in receptor levels or phenotypic characteristics that define these "VEGF-sensitive" cells. We investigated the idea that VEGFR2 levels may be altered by stiffness but discovered that the levels remained constant regardless of stiffness. We further explored the size and shape of the cells within the various clusters to determine if these characteristics were linked to responsiveness. Previous studies indicated that cell shape itself can feedback and influence the stiffness of the actual cells on the matrix[36]. Others have noted that alterations in endothelial cell shape are linked to the cellular release of chemotactic factors and the consequent recruitment of monocytes in *in vivo* models[57]. Indeed, classic studies using *in vitro* 2D polystyrene cell culture systems identified distinct morphological phenotypes of tip cells with long thin lamellipodia compared to more bulky stalk cells[31]. In the present study we observed that the high responders are statistically smaller than the bulk responders at low doses of VEGF. The alteration in size was largely due to decreased length of the minor axis indicating a narrowing of the cells. At higher doses of VEGF, there was no significant difference in size between high responders and low responders. Together, these findings indicate that at low doses of VEGF high responders were morphologically different from bulk responders, but at high doses of VEGF, cells of any shape or size could overcome a threshold allowing them to become a high responder. These findings were not due to an increase in initial VEGFR2 on the smaller cells, in fact we found a slight positive

correlation in cell size and receptor number, indicating as cell surface area increases there is a proportional increase in the amount of receptor. Even though total VEGFR2 number did not appear to vary, it is possible that changes in VEGF-mediated signaling in cells as a function of stiffness or shape are the result of alterations in VEGFR2 internalization and/or recycling. While we did not investigate these possibilities in the present study, changes in VEGF internalization rate in vessels of the retina have been linked to altered cell outputs and responses to VEGF[58].

Two distinct phenotypes of endothelial cells have been reported *in vivo* with respect to VEGF responsiveness – tip cells and stalk cells. Both tip and stalk cells are known to respond to VEGF via VEGFR2 leading to distinct endpoints with tip cells being induced to migrate forward leading to outward sprouting and growth while stalk cells are stimulated to proliferate developing the lumen behind. We previously demonstrated cells on the leading edge of a stimulus are capable of the greatest magnitude of calcium mobilization[59]. Thus it is possible that our distinct subgroups are reflective of these two sub-types of endothelial cells[31]. In this paradigm, the high responders take on the tip cell, leading edge, migratory role and the bulk responders act as stalk cells with a slow steady VEGF activation.

Materials and Methods:

Forty percent acrylamide and two percent bis-acrylamide solutions, and ammonium persulfate were purchased from BioRad (Hercules, CA). Phosphate buffered saline (PBS) (10x) was purchased from Gibco (Grand Island, NY). Gluteraldhyde was purchased from Sigma-Aldrich (Natick, MA). Human fibronectin was from Millipore (Billerica, MA). TEMED and coverslips were acquired from Fisher Scientific (Pittsburgh, PA). Total fibronectin antibody 610077 was from BD Biosciences (San Jose, CA), and TMB Microwell Peroxidase was from KPL (Gathersburg, MD). Cell culture reagents, including fetal bovine serum (FBS), calf serum, trypsin EDTA, Dulbecco's modified Eagle's medium, penicillin streptomycin cocktail, and L-glutamine, were purchased from Corning (Tewksbury, MA). Fn-depleted fetal bovine serum was made using gelatin-agarose (Sigma-Aldrich (Natick, MA)) as previously described[60]. Fluo-3 AM was acquired from Life Technologies (Carlsbad, CA). Human recombinant

$VEGF_{165}$ was obtained from R&D Systems via NCI Bulk Cytokine and Monoclonal Antibody Preclinical Repository (Frederick, MD). Matlab (Mathworks, Natick, MA) segmentation scripts were written in version 2009b. Antibodies for staining Fn and Rat Tail Type-1 Collagen were from Abcam and Rockland respectively. Flow cytometry reagents include the antibody to total VEGFR2 (Cell Signaling), Alexafluor A488 (Invitrogen), fixation and permeability kit (eBioscience), and FACS buffer (BD Biosciences).

Gels: Various stiffness polyacrylamide gels (4, 25, and 125 kPa) were produced using a sandwich methodology developed previously[14, 61]. Briefly, glass coverslips were cleaned with 0.1 N NaOH and washed with distilled water. After drying, coverslips were coated with various concentrations of fibronectin (Fn) protein, depending on the corresponding stiffness, in order to produce a uniform density of Fn on the surface of all gels. After drying the coverslips under vacuum at 4°C, they were washed and dried a second time. A second set of coverslips was treated with 3-aminopropyltrimethoxysilane, allowed to dry, washed several times with distilled water and then treated with 0.5% glutaraldehyde for thirty minutes. Glutaraldehyde was removed, coverslips were washed several times with distilled water, and they were stored in water until ready for use. Polyacryalamide gel mixture (0.1 ul/mm^2) was added to each 3-Aminopropyltrimethoxysilanecoated coverslip[14, 61]. A corresponding Fn coated coverslip was added to the top and gels were allowed to polymerize under vacuum at 4°C for 1 hr at which point the Fn on the top coverslip was successfully transferred, without the aid of NHS-ester, to the covalently linked gel below. Gels were washed in PBS, quenched in sterile 3% BSA-PBS for 1 hr and then washed again with PBS prior to cell seeding.

Gel Protein Verification: Fn-ELISAs were conducted to verify that the density of Fn on the gel surfaces was consistent across the tested stiffness conditions. Known concentrations of Fn were adsorbed to polystyrene surfaces that were the same size of the gels in order to establish standard curves. Gels were fixed for 20 minutes at 4°C in 4% paraformaldehyde in PBS. After fixation, samples were washed in tris buffered saline (TBS) and then incubated in 3% bovine serum albumin (BSA) TBS for 1 hr to block non-

specific sites. After blocking, gels were incubated with BD total Fn primary antibody for 1 hour at a 1:10000 dilution in 3% BSA-PBS, then washed with TBS prior to treatment with a Jackson Laboratories HRP linked secondary antibody to mouse at 1:5000 for 1 hour in 3% BSA-PBS. Finally, samples were washed several times in 0.1% TBS-Tween and TBS prior to 3,3',5,5'-tetramethylbenzidine (TMB) substrate reaction. The absorbances of multiple samples from each well were measured using a 96-well OptiMax plate reader (Molecular Devices). Background A550 readings were subtracted from sample A450 readings. Fibronectin levels were calculated based on the standard curve.

Cell Culture: Bovine Aortic Endothelial Cells (BAECs) (passage 6-16) were used for all experiments. Cells were maintained in DMEM supplemented with 10% calf serum, 1% penicillin/streptomycin cocktail and 1% L-glutamine. BAECs were prepared by washing several times with phosphate buffered saline (PBS) followed by trypsinization of cell sheets. Trypsin was inhibited with DMEM supplemented with 10% Fn-depleted serum. Cells were seeded at 21,000 cells/cm^2 in the Fn-depleted serum. After 24 hrs in culture, the cells were washed once with PBS and fresh 0.5% fibronectin depleted serum was added for the remaining 24 hrs prior to experimentation. All experiments were conducted with cells at 50-70% confluence to maintain consistent levels of cell-cell contacts, which are known to be able to inhibit VEGF activation and cell-ECM specific responses.

Matrix Staining: After 3 days in culture, BAEC cells were fixed with 4% paraformaldehyde PBS for 20 minutes on ice. Solutions were removed, cell layers were washed with PBS 3x prior to permeabilization with 0.1% triton-x 100. Cells were washed again 3x with PBS and then blocked with 3% BSA-PBS for 1 hour at RT. BSA-PBS was exchanged for primary antibody (Type 1 Col 1:100 or Fn 1:250) in BSA-PBS for 1 hour at RT. Prior to the addition of secondary antibody the primary antibody was removed with multiple washes with PBS. Secondary antibody (mouse Alexa A488) was added for 1 hour at RT. Samples were washed 3x more with PBS prior to mounting with Vectashield onto slides. Cells were imaged on a Zeiss 700 confocal.

Flow Cytometry Analysis:

Cells were grown on gels functionalized with fn as described above. After 4 days in culture cells were washed briefly with FACS Buffer containing sodium azide to block further metabolic action. Cells were collected after trypsinization of cell sheets with TrypLE. Cell number was measured and the cells were spun down at 200xg for 5 minutes prior to resuspension in FACS buffer. One million cells were placed in each individual tube and the tubes were centrifuged again to remove the wash buffer. Fixative containing permeabilization buffer was added to each tube for 30 minutes at RT. Solutions were spun down and cells were washed 2x in FACS buffer. Cells were spun down, washed 2x with FACS buffer prior to addition of VEGFR2 antibody (1:100) for 1 hour at RT. Samples were once again spun down and resuspended for two more washes prior to the addition of A488 anti-rabbit to each tube (10 ug/ml) for 30 minutes. After incubation, samples were washed 2 more times in FACS buffer and resuspended for FACS analysis. Cells were passed through cell strainers and were analyzed up to 30000 counts per condition. Background absorbance values at 488 nm were subtracted from the VEGFR2 readings.

Calcium Imaging: All calcium imaging was performed, as previously described[33], on a Zeiss Axiovert 100M LSM 510 equipped with an Argon lasers (Thornwood, NY). Samples were washed 2x in HEPES buffer (10 mM HEPES, 137 mM sodium chloride, 5 mM potassium chloride, 4 mM magnesium chloride, 3 mM calcium chloride, and 25 mM glucose). Fluo-3 am was dissolved in DMSO supplemented with 0.02% pluronic acid. Samples were incubated in Fluo-3 am (1%) in HEPES buffer for 20 minutes (stored in the dark at 37°C). After incubation, samples were washed 1x with HEPES buffer and placed in a flow-mounting chamber (Warner Instruments) as previously described[59]. Flow input was adjusted to approximately 40 ul/second so that flow did not stimulate cells. For each experiment, images were acquired at 789 ms/frame using the argon laser (488 nm). Samples were equilibrated, under HEPES

buffer, for 5 minutes prior to exchanging the control flow buffer to HEPES buffer containing the indicated concentration of VEGF. Experiments lasted 10-15 minutes.

Post Imaging Analysis:

Segmentation: MATLAB cell segmentation was conducted using a method modified from a Mathworks Engineering blog[62]. Briefly, to provide the best average cell representation, the first 50 frames of the treatment were added together. Contrast was enhanced and cell areas were enhanced to optimize perimeter identification. After identifying individual perimeters, the cell nuclei, or minima of each cell were identified. Marked areas containing both a nuclei and a cell perimeter were counted as individual cells[33]. Figure 1 provides step-by-step description of this critical step in analysis.

Data analysis: The software script was written to address many population based outputs and single cell analysis parameters. For all analysis, the segmented cell outlines were utilized to break each image into individual cells that were quantified using a pre-defined MATLAB function, "regionprops". The regionprops function is able to assess cell area, pixel intensities, centroid location, and a variety of other parameters. Utilizing this ability, we were able to calculate the individual cell intensity during treatment and correct it for its own individual background as averaged throughout the first 50 frames of control analysis. This correction minimizes the effect of any cells that may be pre-actived or "primed" to respond prematurely prior to treatment.

Normalized intensity: The normalized intensity is the average intensity in which each cell is further normalized (divided by) its own individual background. The values are represented as percentages. Our population based cell traces represent at least 7-11 biological replicates. Any run where the average normalized maximums were two times greater or less than the maximum of the average normalized intensity for all other runs was pre-excluded from the analysis.

Percent activated: We considered any cells with intensity values over the 95th percentile of cell intensities in the background frames to be considered activated. These frames represent population-based averages of the number of cells activated on each frame.

Number of maximums: An open source peak detection script (PEAKDET, Billauer) was utilized to identify individual local maximum that occurred, separated by a pre-defined distance, in each cell over time.

Hierarchical Clustering: Hierarchical clustering was completed on portions of the cell traces. Cells were clustered and displayed as a clustergram heatmap. The cells from each cluster were averaged together to create visualizations of the cell traces. Activation time was chosen as the time point, after the 50 control frames, in which the normalized intensity value for the trace was above 3%. The deactivation point was chosen as the time in which the cell traces arrived at their maximum. Activation and deactivation rates were calculated by creating a linear best-fit approximation of regions between activation and deactivation time (activation rate) and deactivation time and the end of the run (deactivation rate). Figure 4 provides a visual representation of these calculated values.

Statistical Analysis:

All data presented were generated from 7-11 biological replicates for each stiffness and VEGF dose treatment condition (12 conditions in total). Approximately 80 cells were analyzed from each sample at ~800 separate treatment time points. The coefficient of variation (absolute mean from a run/standard deviation) for each treatment was averaged together. For the coefficient of variation and any other condition in which we were considering the statistical significance between treatment groups we utilized a student's two-sided T-test for unequal variance with alpha set at 0.05. For experiments in which we were comparing groups of data within one experiment (i.e., high responders to bulk responders from the same experimental run), we used a one sided pairwise t-test to test for significance change in size at alpha 0.05.

Conclusion:

We found that endothelial cell responsiveness to VEGF could be tuned to the stiffness of the ECM resting below the cells. A new analytical tool was developed that allows for individual cell analysis, which identified an interesting concentration sensor and two distinct groups of responding cells within each treatment condition. Our high responding group of endothelial cells was highly sensitive to VEGF at all

concentrations and presented with an altered, more compact cell shape, which may correlate with migratory, highly active tip cells. Ultimately our study provides insight into how signaling dynamics, cell heterogeneity, and microenvironment influence tissue regeneration, which may have applications in engineering replacement tissues and the development of therapies to direct tissue repair in response to injury and disease.

Acknowledgements: Thank you to Albert Lee for your assistance in developing our calcium imaging methods, Timothy Sack for your advice in the MATLAB code generation, and Gregory Teicher for your proofing of the manuscript.

Bibliography:

1. P. O. Bonetti, *Arteriosclerosis, Thrombosis, and Vascular Biology*, 2002, **23**, 168-175.
2. F. U. S. Mattace-Raso, T. J. M. van der Cammen, A. Hofman, N. M. van Popele, M. L. Bos, M. A. D. H. Schalekamp, R. Asmar, R. S. Reneman, A. P. G. Hoeks, M. M. B. Breteler and J. C. M. Witteman, *Circulation*, **113**, 657-663.
3. M. P. Jacob, *Biomedicine & Pharmacotherapy*, 2003, **57**, 195-202.
4. G. E. Davis and D. R. Senger, *Circ Res*, 2005, **97**, 1093-1107.
5. J. Li, Y. P. Zhang and R. S. Kirsner, *Microscopy research and technique*, 2003, **60**, 107-114.
6. S. J. Zieman, V. Melenovsky and D. A. Kass, *Arteriosclerosis, Thrombosis, and Vascular Biology*, 2005, **25**, 932-943.
7. P. Tracqui, A. Broisat, J. Toczek, N. Mesnier, J. Ohayon and L. Riou, *Journal of structural biology*, 2011, **174**, 115-123.
8. H. N. Hayenga, A. Trache, J. Trzeciakowski and J. D. Humphrey, *Journal of vascular research*, 2011, **48**, 495-504.
9. T. Matsumoto, H. Abe, T. Ohashi, Y. Kato and M. Sato, *Physiological Measurement*, 2002, **23**, 635.
10. J. Peloquin, J. Huynh, R. M. Williams and C. A. Reinhart-King, *Journal of Biomechanics*, 2011, **44**, 815-821.
11. R. G. Wells, *Hepatology*, 2008, **47**, 1394-1400.
12. F. Guilak, D. M. Cohen, B. T. Estes, J. M. Gimble, W. Liedtke and C. S. Chen, *Cell Stem Cell*, 2009, **5**, 17-26.
13. J. Huynh, N. Nishimura, K. Rana, J. M. Peloquin, J. P. Califano, C. R. Montague, M. R. King, C. B. Schaffer and C. A. Reinhart-King, *Sci Transl Med*, 2011, **3**, 112ra122.
14. O. V. Sazonova, K. L. Lee, B. C. Isenberg, C. B. Rich, M. A. Nugent and J. Y. Wong, *Biophysical Journal*, 2011, **101**, 622-630.
15. J. A. Wood, N. M. Shah, C. T. McKee, M. L. Hughbanks, S. J. Liliensiek, P. Russell and C. J. Murphy, *Biomaterials*, 2011, **32**, 5056-5064.
16. K. Bhadriraju and L. K. Hansen, *Experimental Cell Research*, 2002, **278**, 92-100.

17. B. Trappmann, J. E. Gautrot, J. T. Connelly, D. G. T. Strange, Y. Li, M. L. Oyen, M. A. Cohen Stuart, H. Boehm, B. Li, V. Vogel, J. P. Spatz, F. M. Watt and W. T. S. Huck, *Nat Mater*, 2012, **11**, 642-649.
18. M. Mitsi, K. Forsten-Williams, M. Gopalakrishnan and M. A. Nugent, *Journal of Biological Chemistry*, 2008, **283**, 34796-34807.
19. E. S. Wijelath, S. Rahman, M. Namekata, J. Murray, T. Nishimura, Z. Mostafavi-Pour, Y. Patel, Y. Suda, M. J. Humphries and M. Sobel, *Circ Res*, 2006, **99**, 853-860.
20. B. Hubbard, J. A. Buczek-Thomas, M. A. Nugent and M. L. Smith, *Matrix Biology*, 2014, **34**, 124-131.
21. A. L. Goerges and M. A. Nugent, *Journal of Biological Chemistry*, **279**, 2307-2315.
22. E. S. Wijelath, J. Murray, S. Rahman, Y. Patel, A. Ishida, K. Strand, S. Aziz, C. Cardona, W. P. Hammond, G. F. Savidge, S. Rafii and M. Sobel, *Circulation Research*, 2002, **91**, 25-31.
23. T. T. Chen, A. Luque, S. Lee, S. M. Anderson, T. Segura and M. L. Iruela-Arispe, *The Journal of Cell Biology*, 2010, **188**, 595-609.
24. A. R. Ramjaun and K. Hodivala-Dilke, *Int J Biochem Cell Biol*, 2009, **41**, 521-530.
25. E. A. Phelps and A. J. Garcia, *Regen Med*, 2009, **4**, 65-80.
26. M. L. Koransky, R. C. Robbins and H. M. Blau, *Trends Cardiovasc Med*, 2002, **12**, 108-114.
27. P. Carmeliet, *Nature*, 2005, **438**, 932-936.
28. A. K. Olsson, A. Dimberg, J. Kreuger and L. Claesson-Welsh, *Nature reviews. Molecular cell biology*, 2006, **7**, 359-371.
29. W. C. Aird, *Cold Spring Harbor perspectives in medicine*, 2012, **2**, a006429.
30. W. C. Aird, *Circ Res*, 2007, **100**, 158-173.
31. H. Gerhardt, M. Golding, M. Fruttiger, C. Ruhrberg, A. Lundkvist, A. Abramsson, M. Jeltsch, C. Mitchell, K. Alitalo, D. Shima and C. Betsholtz, *The Journal of Cell Biology*, 2003, **161**, 1163-1177.
32. S. Arima, K. Nishiyama, T. Ko, Y. Arima, Y. Hakozaki, K. Sugihara, H. Koseki, Y. Uchijima, Y. Kurihara and H. Kurihara, *Development*, 2011, **138**, 4763-4776.
33. A. Lee, K. Derricks, M. Minns, S. Ji, C. Chi, M. A. Nugent and V. Trinkaus-Randall, *Am J Physiol Cell Physiol*, 2014, **306**, C972-985.
34. O. V. Sazonova, B. C. Isenberg, J. Herrmann, K. L. Lee, A. Purwada, A. D. Valentine, J. A. Buczek-Thomas, J. Y. Wong and M. A. Nugent, *Matrix biology : journal of the International Society for Matrix Biology*, 2015, **41**, 36-43.
35. F. J. Byfield, R. K. Reen, T. P. Shentu, I. Levitan and K. J. Gooch, *J Biomech*, 2009, **42**, 1114-1119.
36. S.-Y. Tee, J. Fu, Christopher S. Chen and Paul A. Janmey, *Biophysical Journal*, 2011, **100**, L25-L27.
37. C. A. Reinhart-King, M. Dembo and D. A. Hammer, *Biophys J*, 2008, **95**, 6044-6051.
38. J. P. Califano and C. A. Reinhart-King, *Cell Mol Bioeng*, 2010, **3**, 68-75.
39. A. Ambesi and P. J. McKeown-Longo, *Journal of Cell Science*, 2014, **127**, 3805-3816.
40. M. M. Martino, P. S. Briquez, E. Guc, F. Tortelli, W. W. Kilarski, S. Metzger, J. J. Rice, G. A. Kuhn, R. Muller, M. A. Swartz and J. A. Hubbell, *Science*, 2014, **343**, 885-888.
41. R. G. da Silva, B. Tavora, S. D. Robinson, L. E. Reynolds, C. Szekeres, J. Lamar, S. Batista, V. Kostourou, M. A. Germain, A. R. Reynolds, D. T. Jones, A. R. Watson, J. L.

Jones, A. Harris, I. R. Hart, M. L. Iruela-Arispe, C. M. DiPersio, J. A. Kreidberg and K. M. Hodivala-Dilke, *The American Journal of Pathology*, 2010, **177**, 1534-1548.
42. S. De, O. Razorenova, N. P. McCabe, T. O'Toole, J. Qin and T. V. Byzova, *Proc Natl Acad Sci U S A*, 2005, **102**, 7589-7594.
43. B. P. Eliceiri, *Circulation Research*, 2001, **89**, 1104-1110.
44. H. Hutchings, N. Ortega and J. Plouët, *The FASEB Journal*, 2003, DOI: 10.1096/fj.02-0691fje.
45. G. Serini, D. Valdembri and F. Bussolino, *Exp Cell Res*, 2006, **312**, 651-658.
46. M. Simons, *Physiology*, 2012, **27**, 213-222.
47. D.-A. Lacorre, E. S. Baekkevold, I. Garrido, P. Brandtzaeg, G. Haraldsen, F. Amalric and J.-P. Girard, *Blood*, 2004, **103**, 4164-4172.
48. M. E. Gerritsen, *Biochemical Pharmacology*, 1987, **36**, 2701-2711.
49. E. Batchelor, A. Loewer and G. Lahav, *Nat Rev Cancer*, 2009, **9**, 371-377.
50. L. O. Murphy, J. P. MacKeigan and J. Blenis, *Mol Cell Biol*, 2004, **24**, 144-153.
51. S. Traverse, N. Gomez, H. Paterson, C. Marshall and P. Cohen, *Biochem J*, 1992, **288**, 351-355.
52. S. Sasagawa, Y. Ozaki, K. Fujita and S. Kuroda, *Nat Cell Biol*, 2005, **7**, 365-373.
53. C. Cohen-Saidon, A. A. Cohen, A. Sigal, Y. Liron and U. Alon, *Mol Cell*, 2009, **36**, 885-893.
54. R. E. Dolmetsch, R. S. Lewis, C. C. Goodnow and J. I. Healy, *Nature*, 1997, **386**, 855-858.
55. J. E. Purvis and G. Lahav, *Cell*, 2013, **152**, 945-956.
56. M. T. Yang, D. H. Reich and C. S. Chen, *Integrative biology : quantitative biosciences from nano to macro*, 2011, **3**, 663-674.
57. L. Indolfi, A. B. Baker and E. R. Edelman, *Biomaterials*, 2012, **33**, 7019-7027.
58. M. Nakayama, A. Nakayama, M. van Lessen, H. Yamamoto, S. Hoffmann, H. C. Drexler, N. Itoh, T. Hirose, G. Breier, D. Vestweber, J. A. Cooper, S. Ohno, K. Kaibuchi and R. H. Adams, *Nat Cell Biol*, 2013, **15**, 249-260.
59. I. Weinger, V. Klepeis and V. Trinkaus-Randall, *Purinergic Signalling*, 2005, **1**, 281-292.
60. E. Engvall and E. Ruoslahti, *International Journal of Cancer*, 1977, **20**, 1-5.
61. S. R. Polio, K. E. Rothenberg, D. Stamenovic and M. L. Smith, *Acta Biomater*, 2012, **8**, 82-88.
62. E. Steve, *Steve on Image Processing*, 2006.

Figure 1: Progression of the MATLAB algorithm for cell segmentation and identification. A. Import the first control slide. **B.** Add up the first 50 background slides, then adjust the contrast so that the cells are sufficiently bright. **C.** Utilize a function from the MATLAB library to identify cluster perimeters. **D.** Couple the previously identified perimeters with the local minima or nuclei. New segmentations are created between areas with two minima and one perimeter. Processed cells require both a minima and a perimeter. **E.** Number the cells and display for the user to critique the segmentation routine. **F.** Read in all un-processed slides. Use the segmented cells as a mask to identify areas of cell intensities and characteristics.

Figure 2: Characteristics of polyacrylamide gel experimental system. A. Quantification of fibronectin on the surface of the gels prior to cell seeding. **B.** Images of fibronectin matrices 4 days after BAEC growth on the three different stiffness gels (4, 25, 125 kPa). The 4th panel labeled Col indicates BAEC matrix staining of type 1 rat-tail collagen staining on glass after 3 days in culture.

Figure 3: VEGF activation of calcium signaling in BAECs. Population based outputs from MATLAB quantification of BAECs stimulated with the indicated concentration of VEGF are shown. Each measurement represents a composite of 7-11 runs from at least 2-3 independent experiments. All measurements were conducted on three stiffness gels, 4 kPa (blue), 25 kPa (red), and 125 kPa (green), with four different concentrations of VEGF (1, 5, 10, and 25 ng/ml). **A.** Normalized intensity output represents an average of individual cell intensities that have been normalized to the average of their individual initial control background. **B.** Percent of cells that are activated over the 95th percentile of background intensity values as a function of time. **C.** Average number of local maxima throughout the observation period.

Figure 4: Definition of calcium response parameters. A model plot is shown to indicate the specific activities/parameters. **A.** At 50 frames into the experiment, flow is switched to buffer containing VEGF. **B.** Activation time is the time at which the normalized intensity of the cell trace reaches 3% over background. **C.** Maximum time is when the overall maximum of the run occurs. **D.** Overall maximum is the intensity at the maximum of the run. **E.** Activation rate is the best-fit linear approximation from the activation time to the maximum time. **F.** Deactivation rate is the best-fit linear approximation from the maximum time to the end of the run.

Figure 5: Hierarchal clustering analysis of normalized intensity of the VEGF response. BAECs on 4, 25, and 125 kPa gels were treated with VEGF and normalized intensity measured. Heatmaps range from -400 (blue) to 400 (dark red). Line plots show the average of all clusters, containing more than three cells. The average of all cells is represented by the bold blue line. The cluster containing the bulk of all cells analyzed is shown highlighted by a bold gold line. The percent of cells in each cluster is listed in each inset legend. Data for VEGF treatments: **A.** 1 ng/ml, **B.** 5 ng/ml, **C.** 10 ng/ml, **D.** 25 ng/ml.

Figure 6: Average cell traces by cluster. Line plots showing the normalized intensity average (thin line), the average normalized intensity of the bulk cluster (medium size line), and the average of the cells not included in the bulk cluster (large line). Experiments are shown for 4kPa (blue), 25 kPa (red), and 125 kPa (green) over four VEGF concentrations: **A.** 1 ng/ml, **B.** 5 ng/ml, **C.** 10 ng/ml, **D.** 25 ng/ml.

Figure 7: Bulk cluster average cell traces. Line plots showing only the largest (bulk) cluster of cells on each stiffness (4 kPa (blue), 25 kPa (red), and 125 kPa (green)) and VEGF concentration: **A.** 1 ng/ml, **B.** 5 ng/ml, **C.** 10 ng/ml, **D.** 25 ng/ml.

Figure 8: Statistic analysis of clustering. A. Coefficient of variation (mean/standard deviation) averaged for all cell treatments (7-11 biological replicates each) and conditions (over 4 VEGF treatments). Parameters are those defined in Figure 4. There is no significant difference between the variation in cell

areas, but there is significant differences between most of the subtypes of the remaining categories. Significance ($\alpha < 0.05$) in reference to the all cells category, is marked with bars.

Figure 9: Cell size is different between clusters. A-C: Average values for cell sizes of bulk responders and high responders +/- SEM. Significance (always $\alpha < 0.05$) is defined as a difference between the high and bulk responder categories for each run (7-11 per stiffness and 3 different stiffness) in a pairwise one-tailed T-test. **D-F:** The average differences between bulk and high responders for each cell size parameter. Significance is defined for differences between concentrations using an unequal variance, two-tailed T-test. **A** and **D:** Area, **B** and **E:** Major Axis, **C** and **F:** Minor Axis

Figure 10: VEGFR2 levels are constant with stiffness. VEGFR2 levels were measured using flow cytometry with an antibody to total VEGFR2. Briefly, cells were suspended from gels, counted, fixed and permeabilized and stained with primary antibody for 1 hour and fluorescent secondary antibody for 30 minutes. Cells were washed and transferred to cell strainer tubes for BD FACS Caliber analysis. Median values reflect the median fluorescent intensity of VEGFR2 staining after correction for secondary only background. The median fluorescence intensity values are provided for cells isolated from gels of each stiffness as well as for cells where the primary VEGFR2 antibody was excluded (secondary only control).

Stiffness	Average # of Cells/Run	Area (μm^2)	Major Axis Length (µm)	Minor Axis Length (µm)
4 kPa	79 +/- 30	556.64 +/- 6.43	34.84 +/- 0.22	18.67 +/- 0.12
25 kPa	70 +/- 12	625.47 +/- 9.10	37.22 +/- 0.28	19.66 +/- 0.15
125 kPa	87 +/- 18	528.87 +/- 5.39	33.90 +/- 0.19	18.39 +/- 0.11

Table 1: Descriptive information regarding the geometry and size of cells analyzed. Area is the quantitative area of the region segmented, it is a true value, not an approximation based on a relative diameter. For each region, an artificial ellipse with the same second moments of the cell is created over the segmented cell. The major axis length and minor axis length are reflective of this ellipse. The number of cells per run is represented with +/- standard deviation. The remaining characteristics are given as +/- standard error of the mean. All areas and relative cell lengths were significant when compared to each other, except for no significant difference between the minor axis length of the 4Kpa and 125 kPa samples.

Stiffness	Treatment	Activation Time (min)	Maximum Time (min)	Activation Rate	Deactivation Rate	Maximum	% Activated Maximum
4 kPa	1 ng/ml	3.00	10.00	7.16	-2.46	51.2	60.68
	5 ng/ml	2.07	5.96	25.8	-5.3	96.88	68.58
	10 ng/ml	0.68	5.60	18.95	-5.23	74.47	60.79
	25 ng/ml	1.93	4.68	28.06	-6.89	77.41	63.02
25 kPa	1 ng/ml	3.56	10.27	9.78	-1.54	63.10	63.21
	5 ng/ml	2.39	7.49	13.33	-2.33	69.80	63.07
	10 ng/ml	1.76	5.60	31.63	-4.48	116.93	72.01
	25 ng/ml	1.04	5.37	24.42	-4.98	90.37	63.88
125 kPa	1 ng/ml	3.84	9.98	7.26	-1.95	47.93	54.36
	5 ng/ml	2.64	8.36	9.11	-0.67	56.51	59.94
	10 ng/ml	2.16	7.02	12.15	-3.43	64.57	59.76
	25 ng/ml	2.06	5.62	14.18	-4.03	52.07	51.53

Table 2: Descriptive information on the cell traces provided in Figure 3. Information on overall trace maximum, activation time, deactivation time, and the rate of activation and deactivation is provided for each normalized intensity trace. These values are demonstrated on Figure 3B. Activation rate is the slope of the best-fit linear approximation from the activation time (the first point over 3% normalized intensity) through to the overall maximum. Deactivation rate occurs from the overall maximum time to the end of each run. The percentage maximum number of cells activated for each run is also included.

Stiffness	Treatment	Cluster	Activation Time (min)	Maximum Time (min)	Activation Rate	Deactivation Rate	Maximum
4 kPa	1 ng/ml	Average	3.00	10.0	7.16	-2.46	51.2
	5 ng/ml		2.07	5.96	25.8	-5.3	96.88
	10 ng/ml		0.68	5.60	18.95	-5.23	74.47
	25 ng/ml		1.93	4.68	28.06	-6.89	77.41
	1 ng/ml	Bulk Cluster	5.77	10.39	4.70	-2.01	23.49
	5 ng/ml		3.27	8.32	5.49	-2.54	30.23
	10 ng/ml		3.49	7.92	4.19	-2.09	20.72
	25 ng/ml		2.65	5.02	3.21	-1.66	11.13
	1 ng/ml	High Responder	1.63	8.12	35.91	-12.82	189.80
	5 ng/ml		1.10	5.59	78.40	-18.71	274.07
	10 ng/ml		1.59	5.09	62.42	-14.19	198.59
	25 ng/ml		1.75	4.68	77.06	-18.30	214.09
25 kPa	1 ng/ml	Average	3.56	10.27	9.78	-1.54	63.10
	5 ng/ml		2.39	7.49	13.33	-2.33	69.80
	10 ng/ml		1.76	5.60	31.63	-4.48	116.93
	25 ng/ml		1.04	5.37	24.42	-4.98	90.37
	1 ng/ml	Bulk Cluster	5.68	10.27	6.69	0.49	35.08
	5 ng/ml		4.73	10.50	2.66	0.00	20.02
	10 ng/ml		3.03	9.91	3.82	-7.69	31.51
	25 ng/ml		1.04	6.69	3.99	-1.18	19.23
	1 ng/ml	High Responder	2.87	7.77	33.34	-4.20	151.29
	5 ng/ml		1.89	5.39	69.15	-10.43	211.03
	10 ng/ml		1.63	5.12	88.13	-14.49	286.28
	25 ng/ml		0.66	5.40	64.37	-13.90	231.68
125 kPa	1 ng/ml	Average	3.84	9.98	7.26	-1.95	47.93
	5 ng/ml		2.64	8.36	9.11	-0.67	56.51
	10 ng/ml		2.16	7.02	12.15	-3.43	64.57
	25 ng/ml		2.06	5.62	14.18	-4.03	52.07
	1 ng/ml	Bulk Cluster	6.02	10.14	4.98	0.31	23.08
	5 ng/ml		5.37	10.50	3.03	0	18.77
	10 ng/ml		4.53	9.56	2.80	-2.65	18.20
	25 ng/ml		3.83	6.51	2.93	-1.15	11.43
	1 ng/ml	High Responder	3.23	7.05	32.77	-4.77	121.14
	5 ng/ml		2.02	6.09	51.29	-8.33	188.50
	10 ng/ml		1.73	5.46	60.40	-14.41	212.21
	25 ng/ml		1.52	5.22	59.04	-15.36	193.47

Table 3: Descriptive information on the cell traces provided in Figures 5 and 6. Information on maximum, activation time, deactivation time, and the rate of activation and deactivation is provided for each normalized intensity race. The information is separated by both concentration and the average of all traces, the bulk cluster, and the cells not included in the bulk cluster (ie the high responders).

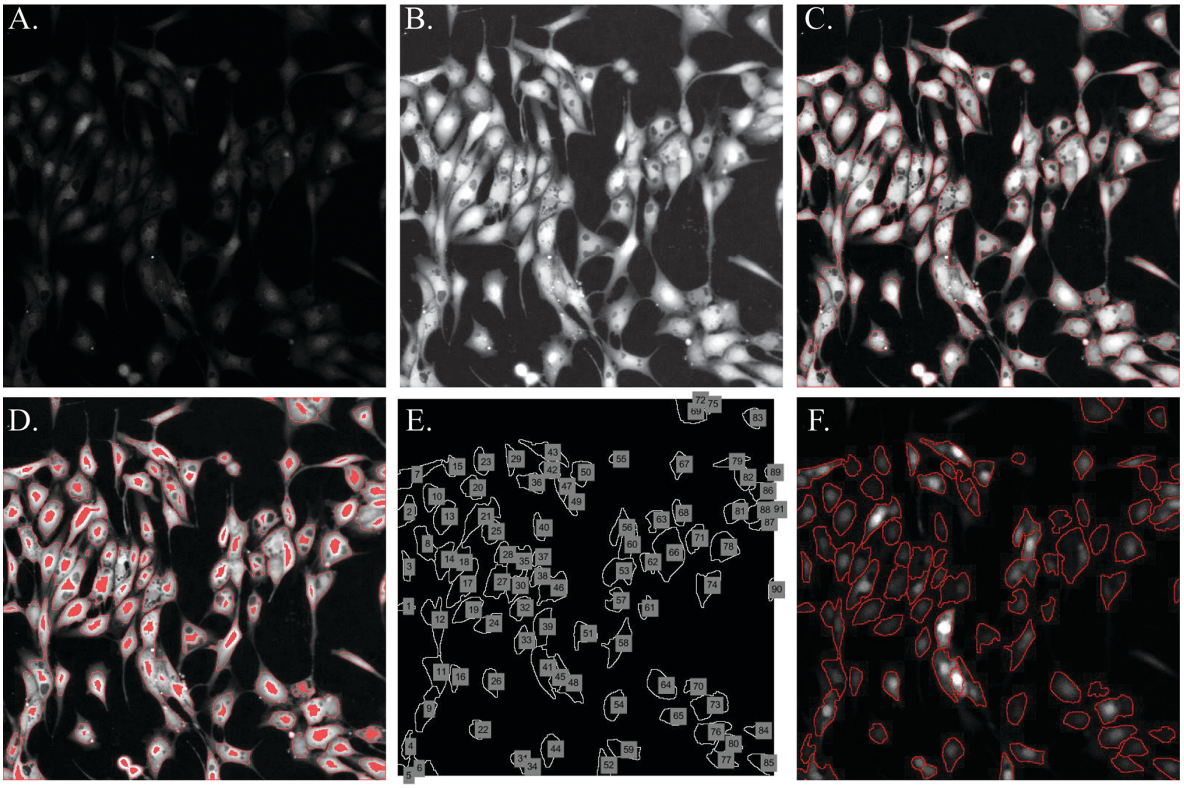

Figure 1

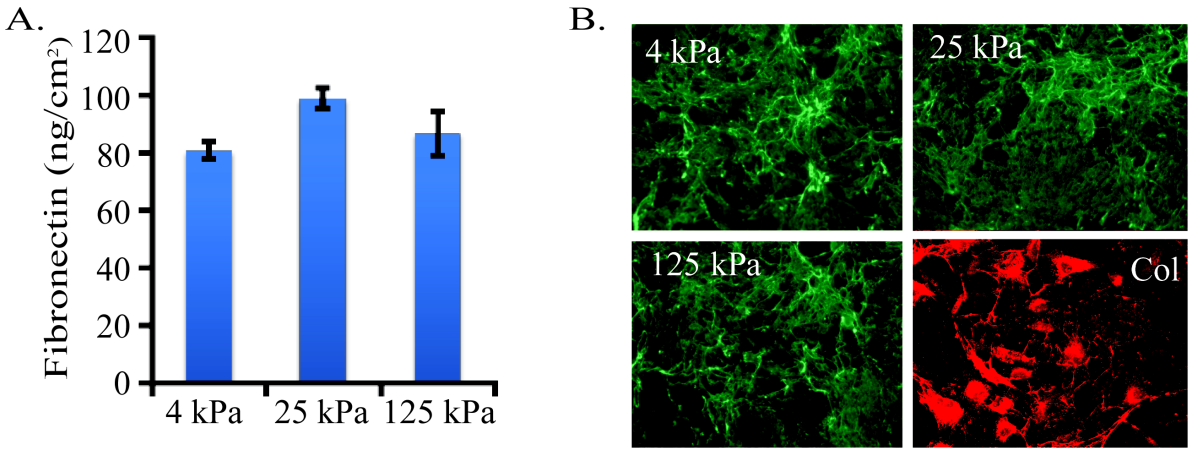

Figure 2

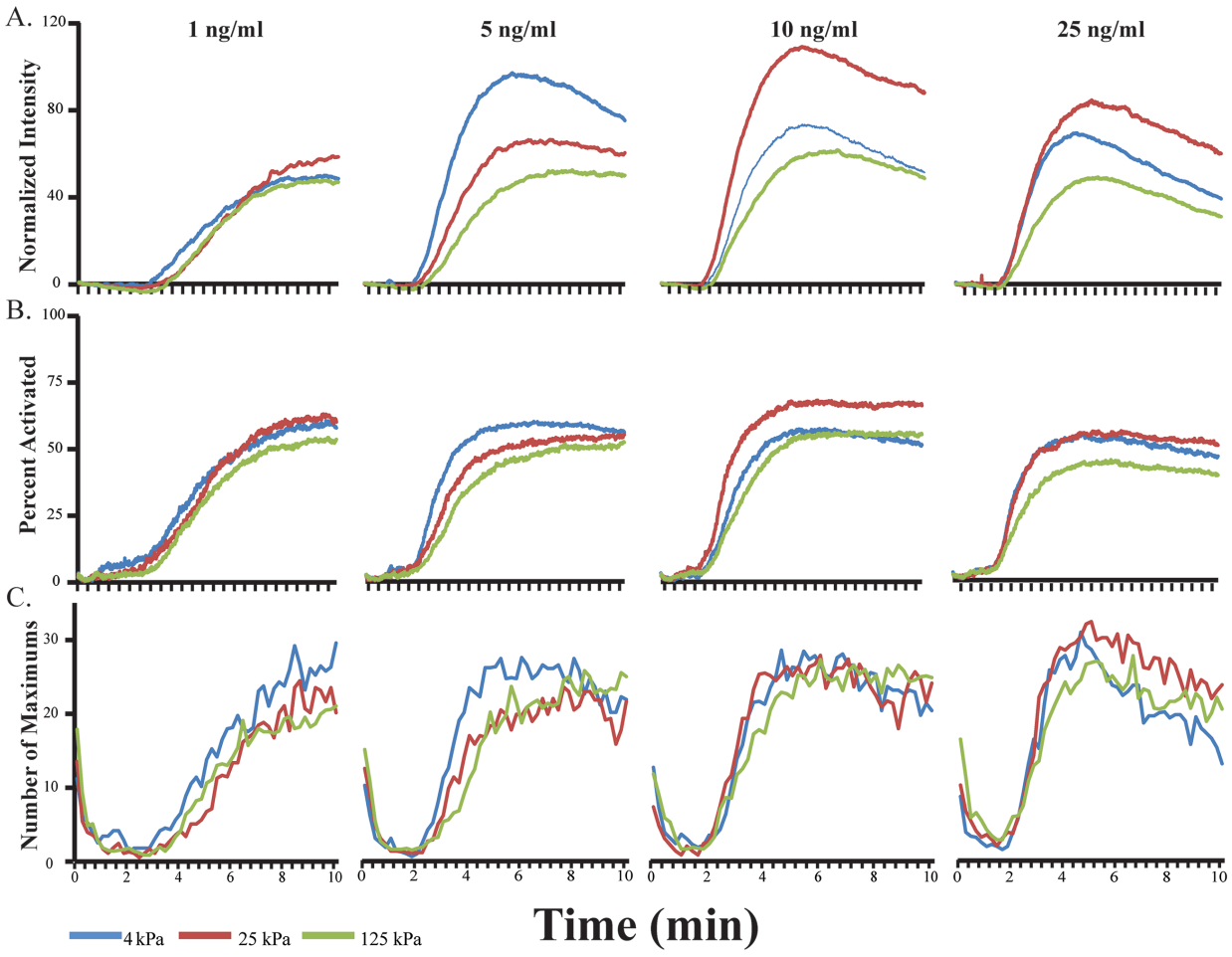

Figure 3

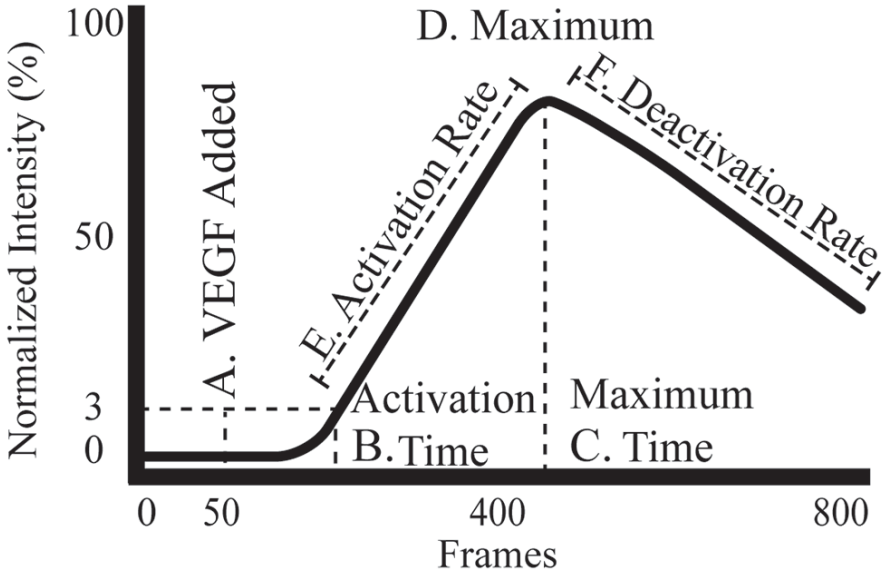

Figure 4

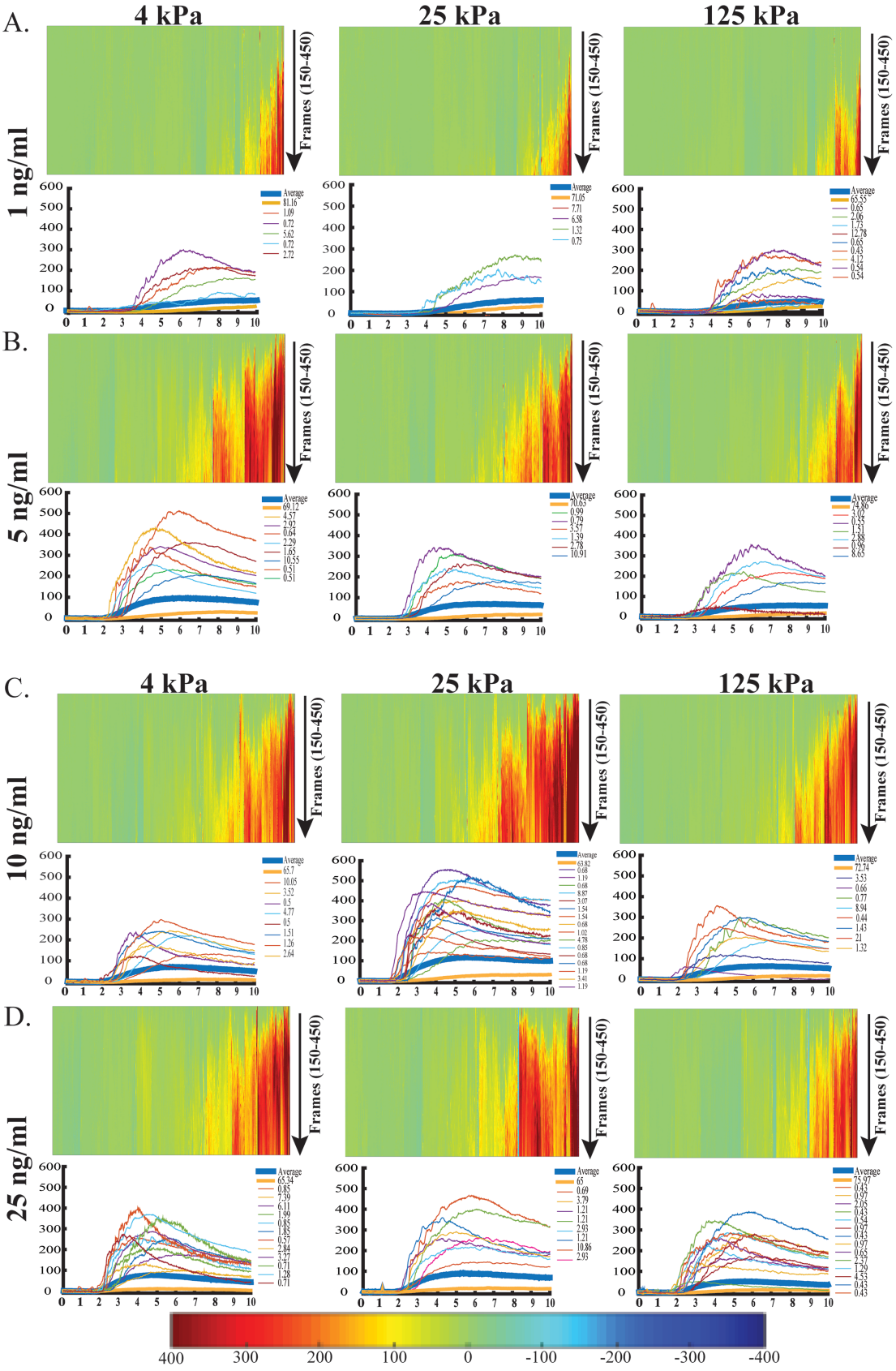

Figure 5

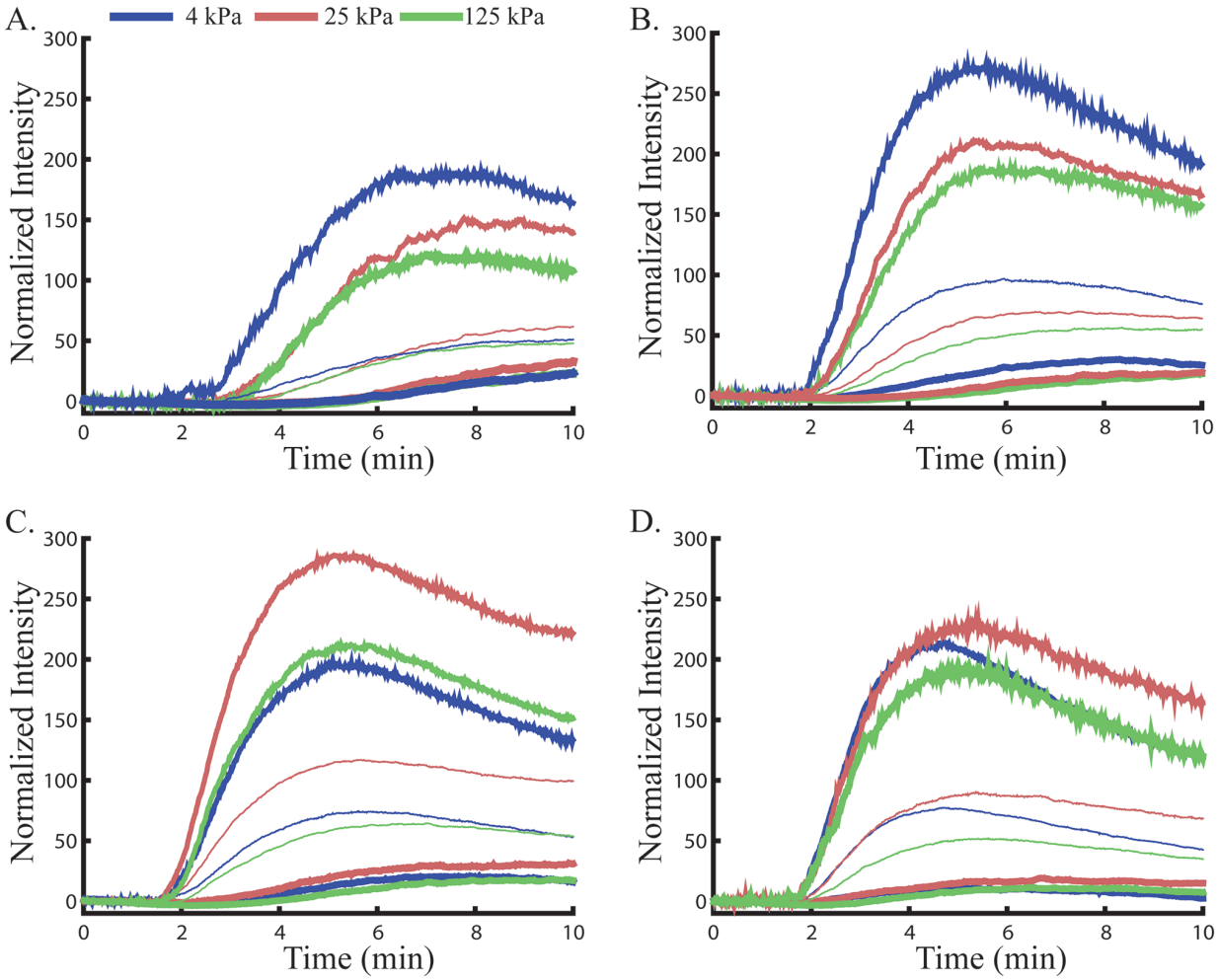

Figure 6

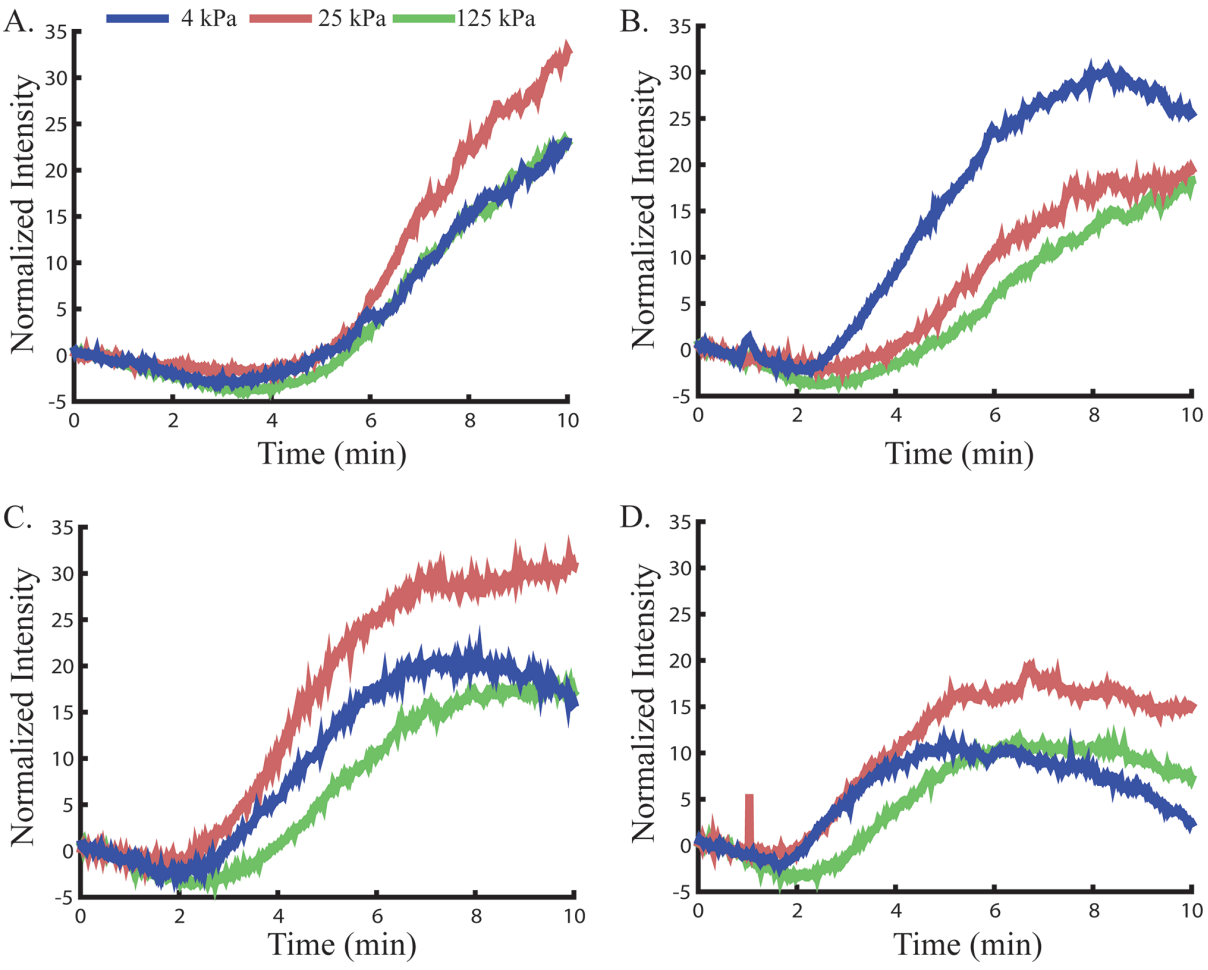

Figure 7

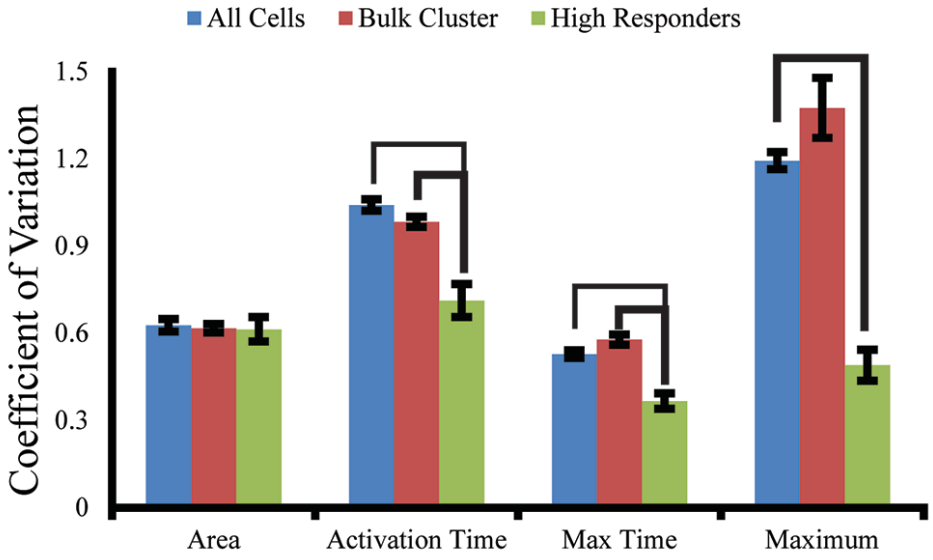

Figure 8

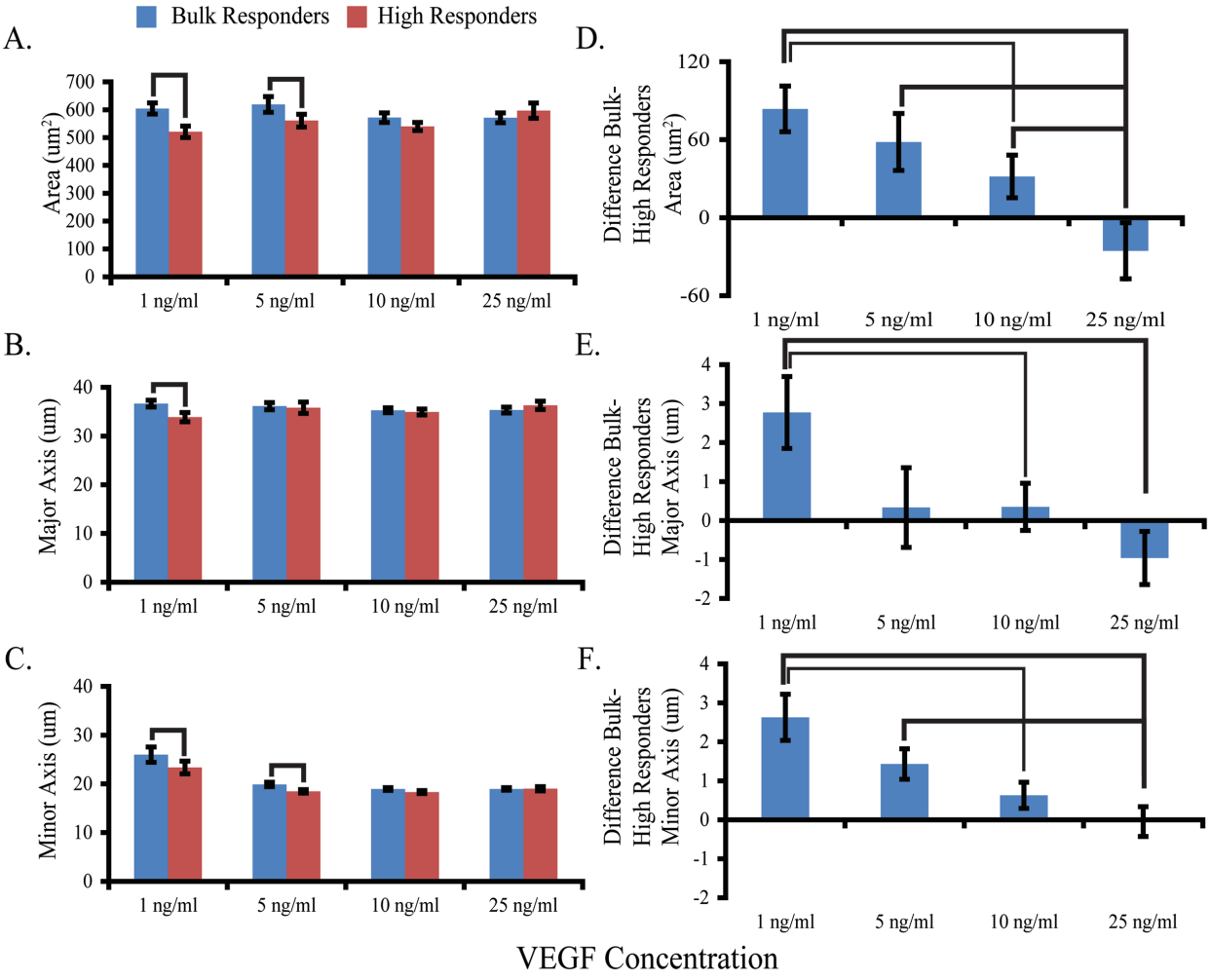

Figure 9

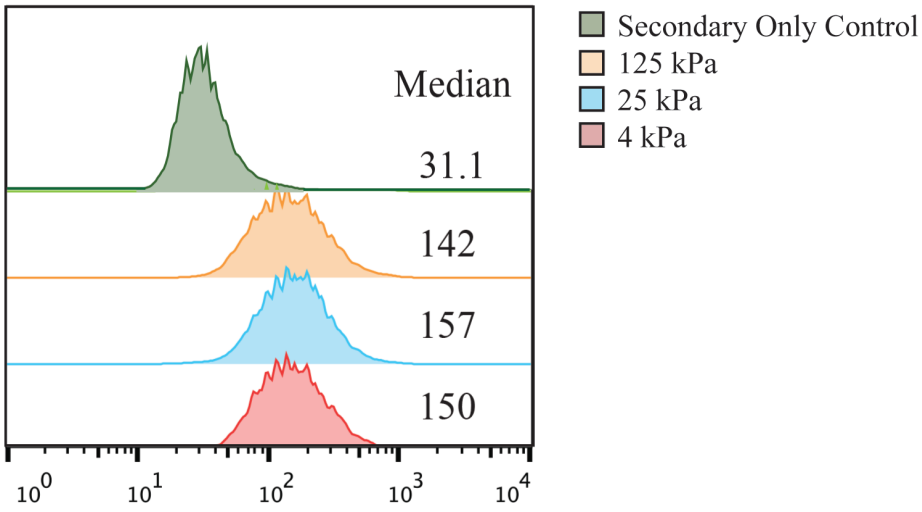

Figure 10